CHINESE OPTICS LETTERS

Vol. 23, No. 3 | March 2025

High-resolution waveguide array-based astronomical spectrograph with cascaded phase modulation

Yunxian Zhong (仲韵贤)[1,2,3], Dong Lin (林 栋)[1,2,3], Biao Xu (徐 彪)[1,2,4], Zhuangzhuang Zhu (朱壮壮)[1,2,3], Xue Tong (童 雪)[1,2,3], Qing Zhong (钟 晴)[1,2,3], Jijun Feng (冯吉军)[5*], and Jinping He (何晋平)[1,2,4**]

[1] Laboratory of Solar and Space Instruments, Nanjing Institute of Astronomical Optics & Technology, Chinese Academy of Sciences, Nanjing 210042, China

[2] CAS Key Laboratory of Astronomical Optics & Technology, Nanjing Institute of Astronomical Optics & Technology, Chinese Academy of Sciences, Nanjing 210042, China

[3] University of Chinese Academy of Sciences, Beijing 100049, China

[4] University of Chinese Academy of Sciences, Nanjing 211135, China

[5] Shanghai Key Laboratory of Modern Optical System, Engineering Research Center of Optical Instrument and System, Ministry of Education, School of Optical-Electrical and Computer Engineering, University of Shanghai for Science and Technology, Shanghai 200093, China

*Corresponding author: fjijun@usst.edu.cn

**Corresponding author: jphe@niaot.ac.cn

Received May 31, 2024 | Accepted August 30, 2024 | Posted Online March 12, 2025

Integrated photonic spectrographs could provide a new generation of low-cost, highly integrated, high-performance optical terminal instruments for astronomical observations. However, these spectrographs still face the challenge of high spectral resolution. In this Letter, we demonstrate a cascaded phase-modulated waveguide array (CPMWA) spectrograph, with designed and measured spectral resolutions of 100,000 and 68,000, respectively. A spectral reconstruction method is proposed to minimize the influence of the phase error induced during the chip fabrication process and increase the spectral contrast to 20 dB. This type of spectrograph demonstrates promising potential for high-resolution spectrum observations in astronomy.

Keywords: astronomical spectrograph; waveguide array; cascaded phase modulation; high spectral resolution; spectrum reconstruction.

DOI: 10.3788/COL202523.031301

1. Introduction

The cost-effectiveness and extreme compactness of integrated photonic devices are advantageous for astronomical observations[1,2], especially in challenging observational scenarios, such as space-based astronomy[3], polar astronomy[4], and massive astronomical spectral surveys[5]. In astrophotonics studies, integrated photonic spectrographs have attracted attention because spectroscopy is one of the most important research methods in astronomy[6].

Various types of integrated photonic spectrographs have been proposed, including arrayed waveguide grating (AWG) spectrographs[7], single-nanowire spectrographs[8], and stationary-wave-integrated Fourier-transform spectrographs[9]. AWG spectrographs have attracted considerable attention[10] because of their various advantages, such as their high optical efficiency, relatively high resolution, high accuracy, large bandwidth[11], and well-established processing techniques.

The first attempted use of an AWG spectrograph for astronomical observations was conducted by Cvetkovic *et al*[12]. Then, the AWG spectrograph was tested on an 8-m Subaru telescope[13]. The spectral resolution was limited to approximately 5,000. To improve the resolution, longer delay lines of the phased array induced by the waveguide arrays are necessary. Stoll *et al.* designed a folded and horseshoe-shaped AWG spectrograph to achieve a resolution of up to 20,000[14,15]. The curvature of the object image plane causes defocus aberration for the off-axis beams, which inevitably decreases the resolution. Zhang *et al.* obtained a resolution of up to 90,000 by introducing a reusable delay-line structure into an AWG spectrograph[16]. However, this approach has a limited bandwidth because wavelength-related directional couplers exist in the chip. The crosstalk is also extremely high, which hinders practical applications[17]. Careful design is still required to increase the delay lines with a compact structure and other parameters that are not significantly affected.

Another problem with high-resolution waveguide-array spectrographs is high-precision micro/nanofabrication[18]. Typically, long waveguides are necessary for obtaining

sufficiently long delay lines and high resolutions. However, random spatial variations of mode propagation constants in the free propagation region (FPR) and random variations of arrayed waveguide optical lengths are inevitable in the micro/nano fabrication process[19]. These induce phase errors in the phased array, which increase the crosstalk and decrease the contrast of the spectrum, especially in the case of high-resolution spectrographs. A refractive index non-uniformity below $\sim 10^{-4}$ is required for the successful fabrication of a high-resolution spectrograph[20]. Piezoelectric[21] and thermo-optic methods have been proposed to correct phase errors after fabrication. Gehl *et al.* used integrated thermo-optic phase shifters to correct the phase error, optimizing the spectral contrast of the AWG with 11 channels to 15 dB[22]. However, the integration of a phase shifter for each waveguide significantly increases the size and cost of the chip[23]. A data post-processing method based on a spectral reconstruction that calculates and corrects the phase errors of each waveguide offers the possibility of the mass production of self-correcting AWG spectrographs.

In this Letter, we developed a high-resolution waveguide-array spectrograph using a cascaded phase modulation structure with designed and measured spectral resolutions of 100,000 and 68,000, respectively. We proposed a data post-processing method to calculate the phase error and reconstruct the spectrum, which improves the spectral contrast to 20 dB.

2. Device Design

The spectral resolution of the waveguide-array spectrograph is given by

$$\delta\lambda = \frac{\lambda^2}{N \times n_g \times \Delta L}, \tag{1}$$

where λ is the center wavelength, n_g is the group index of the waveguides, ΔL is the length difference between neighboring waveguides, and N is the number of waveguides. To increase the spectral resolution for a certain number of waveguides, ΔL should be as large as possible within the limited chip space.

To obtain as high a resolution as possible, we designed the cascaded phase-modulation waveguide-array (CPMWA) spectrograph shown in Fig. 1(a). A star coupler was employed to separate the input light from a single waveguide into waveguide arrays, and a reconfigurable module was used to generate a suitable output end for phase modulation. The cascaded phase modulation structure was then used to generate a sufficient phase difference. Finally, the output of the waveguide array was designed to produce a planar wavefront to minimize off-axis aberrations, which are problematic in traditional AWG structures[14].

A star coupler was used as the beam-splitting element to separate the input waveguide into multiple transmission waveguides through the FPR, as shown in Fig. 1(b). The tapers were used to create smooth transitions between the FPR and subsequent transmission waveguide to minimize coupling

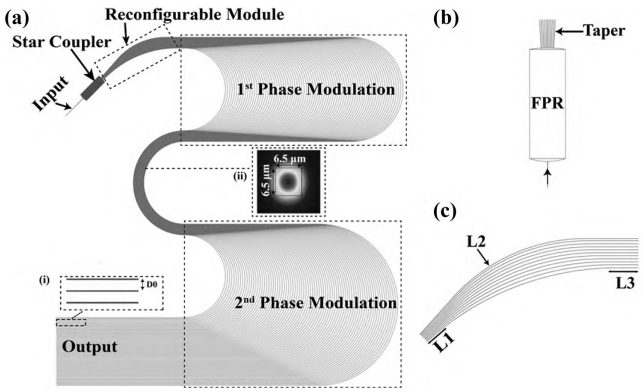

Fig. 1. (a) Schematic diagram of the CPMWA structure. Inset (i) shows variable output waveguide spacing. Inset (ii) shows the design and optical field mode of the waveguide. (b) Schematic diagram of the star coupler. (c) Schematic diagram of the reconfigurable module.

losses through mode matching of the waveguide array and the FPR. Figure 2(a) shows an 80-way split design using a star coupler. By sampling after the output tapered waveguide, the light intensity distribution of the array waveguide was found to be Gaussian, as shown in Fig. 2(b), and the phase of each waveguide was the same. The reconfigurable module can help rearrange the geometry of the waveguide array to a parallel structure from a divergent pattern, which is necessary for efficient light coupling of the star coupler and the waveguide array. As Fig. 1(c) shows, the reconfigurable module consists of straight segments (L1), arc segments (L2), and straight segments (L3). L1 was connected to the end of the star coupler, L2 was used to correct the divergence angle of the waveguide array, and L3 was employed to form a parallel and equally spaced waveguide array structure that was combined with L1 to form a fixed-length difference. The reconfigurable module supplies the phase modulation module with a suitable output end and helps reduce the size of the following structure significantly. This also generates a length difference between adjacent waveguides. However, the value is typically less than 100 μm, which cannot support a high-resolution spectrum. As a result, a phase modulation module is necessary.

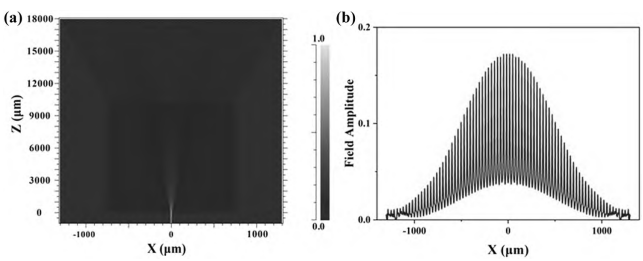

Fig. 2. (a) Electric field amplitude obtained through the beam propagation simulation of the star coupler. (b) The electric field amplitude at the end of the simulated region shows the Gaussian envelope of the illumination pattern of the tapered waveguide as sampled by the waveguide array.

The structure of the phase modulation module is as follows. The first phase modulation structure is set immediately after the reconfigurable module and can generate a length difference of 8 cm, which can support a resolution of 45,000 on a silica platform. To enhance the resolving power to a higher level, another phase modulation (second phase modulation) is added with a U-shaped adapter structure to minimize the negative length difference and structure size. With the two-stage phase modulation demonstrated above, the total length difference can reach 18 cm, and the theoretical spectral resolution can reach 100,000 on a silica platform. According to our calculation, the overall size of the CPMWA chip is only 10% of that of the conventional AWG structure with the same resolution. High resolution can be achieved in smaller sizes using materials with high refractive index differences. Furthermore, multiple structures can be stacked vertically to achieve high resolution with even smaller sizes.

The output section of the CPMWA consists of a series of uniformly distributed waveguide arrays that emit an array of beams with constant phase differences. The primary purpose of this module is to obtain a continuous high-resolution spectrum. To disperse different orders of the spectrum and obtain broadband detection, the geometry of the waveguide array output was designed to be compatible with orthogonal dispersion optics, effectively eliminating spectral overlap. Furthermore, by allowing for an arbitrary adjustment of the spacing D0 between adjacent waveguides, as illustrated in inset (i) of Fig. 1, it is possible to create a customized aperture that is compatible with a wide range of traditional optics.

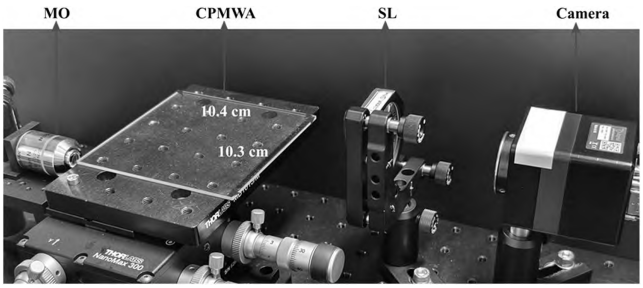

Fig. 3. Experimental setup of the CPMWA spectrograph. MO, microscope objectives; SL, spherical lens.

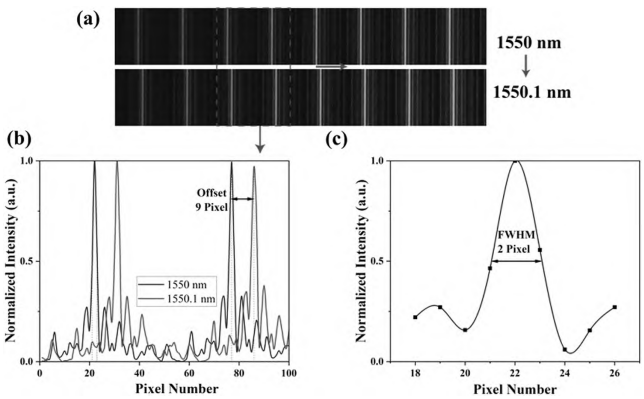

Fig. 4. (a) Captured spectral lines at different wavelengths of the CPMWA spectrograph. (b) Spectrum measured with the CPMWA spectrograph. (c) Measured and fitted spectrum with an FWHM of 2.0 pixels at 1550 nm.

3. Device Fabrication and Characterization

The fabrication of this chip involved photolithography and reactive ion etching on a 6-in wafer. Subsequently, a 12-μm-thick SiO_2 cladding layer was deposited using flame hydrolysis deposition. The CPMWA has an array of 80 single-mode, rectangular buried channel waveguides, each having core dimensions of 6.5 μm × 6.5 μm, as shown in inset (ii) of Fig. 1. The refractive index of the SiO_2 buffer and cladding was 1.4567, and the core refractive index was 1.46 ($\Delta = 0.23\%$) at the central wavelength of 1550 nm. To finalize the process, the chip was diced to dimensions of 10.4 cm × 10.3 cm × 0.1 cm and underwent facet polishing for further refinement.

The CPMWA spectrograph was characterized using the setup illustrated in Fig. 3. A narrow-linewidth laser source (Alnair Labs: TLG-220) was employed, and its output was collimated using a fiber collimator. The collimated light was coupled to the input waveguide using a 10× objective lens. A lens with a focal length of 200 mm was positioned behind the chip to focus the output light on an infrared CCD (Raptor Photonics, Owl-CL-640).

With the setup demonstrated in Fig. 3, a spectrum of two separated wavelengths, 1550.0 and 1550.1 nm, is obtained, as shown in Fig. 4(a). Experimental observations demonstrate that a variation with a 0.1-nm wavelength corresponds to a movement of 9.0 pixels in the spectral image captured by the detector, as shown in Fig. 4(b). Additionally, the full width at half-maximum (FWHM) of the peaks in Fig. 4(c) is approximately 2.0 pixels. Hence, the spectral resolution of the CPMWA spectrograph was calculated as 0.0227 nm, which is equal to 68,282 at a wavelength of 1550 nm.

The measured resolution of the spectrograph is approximately 68% of the theoretical value. The main cause of the decrease in resolution is the incomplete involvement of all waveguides in the multibeam interference. We measured the normalized transmission of 80 waveguides in the CPMWA chip. The data are illustrated in Fig. 5(a). Figure 5(b) shows that more than 35 waveguides do not have sufficient transmission compared with the designed chip. We also calculated the line spread function (LSF) of the CPMWA spectrograph with the theoretical and measured transmission and found that the spectral resolution deteriorated by approximately 70%, as illustrated in Fig. 5(c).

4. Spectrum Reconstruction

As shown in Fig. 4(b), the measured spectral contrast, which is calculated by comparing the secondary peaks with the main peak, is only 5 dB, owing to the large phase error of the phased array caused by imperfect manufacturing. The proposed data

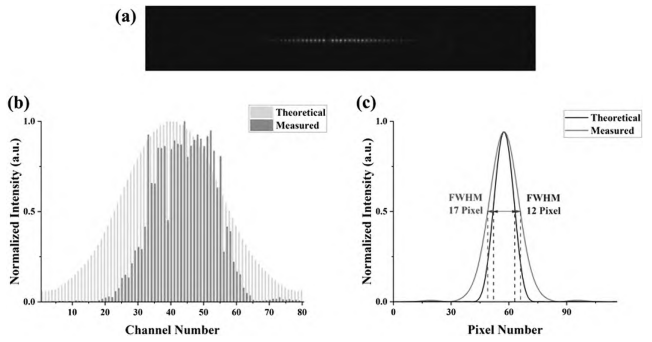

Fig. 5. (a) Near-field images of the output facet of the CPMWA. (b) Normalized light transmission of the 80 waveguides in the CPMWA chip. (c) The line spread function of the CPMWA spectrograph is calculated from the theoretical (blue line) and measured transmission (red line).

post-processing approach addresses this issue. This method involves calculating phase errors and correcting the spectrum to obtain a higher contrast.

First, a model of the CPMWA spectrograph is constructed considering light propagation, multibeam interference, and spectral imaging processes, as shown in Fig. 6(a). The transfer function of the ideal CPMWA chip, denoted by $f(\lambda)$, is determined by the chip design. However, in the real case, phase errors, represented as $\{x_1, x_2, \ldots\}$, where x_i represents the phase error of the ith waveguide, change the transfer function to $f(\lambda; x_1, x_2, \ldots)$. To determine the unknown phase errors of the waveguide array, a series of inputs with different single wavelengths λ_n was applied, and the corresponding multibeam interference pattern S_n was obtained. The phase errors can then be resolved with these data $\{S_1, \lambda_1; S_2, \lambda_2; \ldots\}$, using a basic optimization procedure, expressed as $x = \min_x \sum_{n=1}^{N} |f(\lambda; x_1, x_2, \ldots) - S_n|^2$, where $x = \{x_1, x_2, \ldots\}$, and N represents the number of inputs. The phase error detection process is shown in Fig. 6(b).

Using the phase-error data obtained as described earlier, the spectrum reconstruction was performed using the process shown in Fig. 6(c). For the measured low-contrast spectrum S, an optimization procedure was applied to obtain an optimum intermediate spectrum with an inverse calculation using the

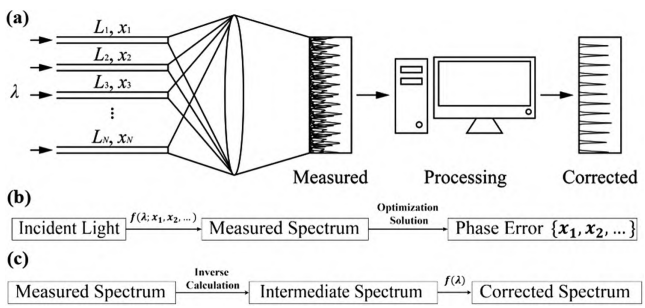

Fig. 6. (a) Spectrum reconstruction overall process. L_i represents the designed length of the ith waveguide. (b) Phase error detection. (c) Spectrum reconstruction process.

model of the CPMWA spectrograph. Since the cross disperser is not arranged in the setup, the input spectrum and that measured with the spectrograph do not have a one-to-one mapping relationship. For example, wavelengths separated by the free spectral range were measured as the same wavelength. Consequently, the intermediate spectrum, which is calculated from the inverse model, possesses all the information of the input spectrum but has a large difference. To solve this problem, we used the intermediate spectrum as the input and applied the model again to obtain the corrected spectrum.

To obtain the transfer function of the real CPMWA chip, 80 single-frequency light beams with different wavelengths were injected into the spectrograph, and the corresponding spectra were measured. Figure 7 illustrates the ideal, measured, and reconstructed spectra. We observed that the spectral contrast

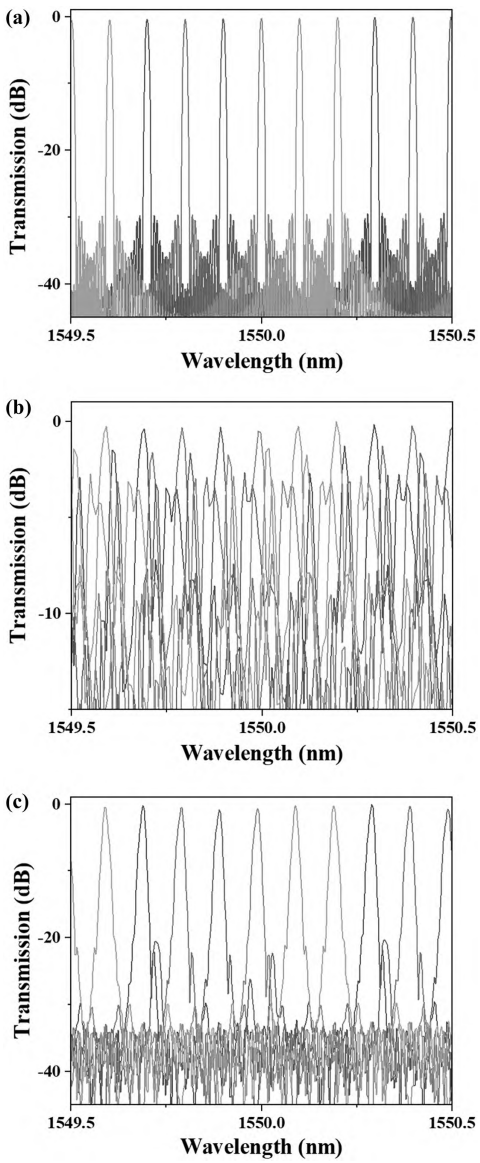

Fig. 7. (a) Ideal spectrum. (b) Measured spectrum. (c) Corrected spectrum, contrast up to 20 dB.

was enhanced to 20 dB using the proposed method. The method does not need complex phase measurement and phase compensation equipment, and only requires one phase error calibration process, which makes the spectrograph more compact and feasible.

5. Conclusion

We have proposed and successfully demonstrated a CPMWA spectrograph with a designed spectral resolution of 100,000 and a measured spectral resolution above 68,000. We proposed a spectral reconstruction method to calculate the phase errors and correct the spectrum to minimize the impact of unavoidable phase errors induced during the chip fabrication process. Using this method, a high-contrast spectrum can be obtained without relying on a high-precision fabrication process. The CPMWA spectrum can be reconstructed by performing only one calibration of the phase errors. Using the approach described above, the spectral contrast of the CPMWA spectrograph was improved to 20 dB. The presented CPMWA spectrograph has potential for applications in high-resolution observing and analyzing of astronomical objects such as stellar and galactic evolution.

Acknowledgements

This work was supported by the National Natural Science Foundation of China (Nos. 11973009, 11933005, U23A20381, 11904232, 11774235, and 61705130), the Jiangsu Provincial Key Research and Development Program (No. BE2023080), the Chinese Academy of Sciences (No. KGFZD-145-23-04-03), the National Key Research and Development Program of China (No. 2022YFE0107400), the Science and Technology Commission of Shanghai Municipality (Nos. 23010503600 and 23530730500), and the Program for Professor of Special Appointment (Eastern Scholar) at Shanghai Institutions of Higher Learning (No. GZ2020015).

References

1. P. Gatkine, S. Veilleux, Y. Hu, *et al.*, "Arrayed waveguide grating spectrometers for astronomical applications: new results," Opt. Express **25**, 17918 (2017).
2. P. Gatkine, S. Veilleux, and M. Dagenais, "Astrophotonic spectrographs," Appl. Sci. **9**, 290 (2019).
3. H. Bradt, *Astronomy Methods: A Physical Approach to Astronomical Observations* (Cambridge University Press, 2003).
4. M. C. McCarthy, K. L. K. Lee, R. A. Loomis, *et al.*, "Interstellar detection of the highly polar five-membered ring cyanocyclopentadiene," Nat. Astron. **5**, 176 (2021).
5. H. Yan, H. Li, S. Wang, *et al.*, "Overview of the LAMOST survey in the first decade," Innovation **3**, 100224 (2022).
6. N. Jovanovic, P. Gatkine, N. Anugu, *et al.*, "2023 Astrophotonics Roadmap: pathways to realizing multi-functional integrated astrophotonic instruments," J. Phys. **5**, 042501 (2023).
7. P. Gatkine, S. Veilleux, Y.-W. Hu, *et al.*, "Development of high-resolution arrayed waveguide grating spectrometers for astronomical applications: first results," in *Advances in Optical and Mechanical Technologies for Telescopes and Instrumentation II* (2016).
8. Z. Yang, T. Albrow-Owen, H. Cui, *et al.*, "Single-nanowire spectrometers," Science **365**, 1017 (2019).
9. E. le Coarer, S. Blaize, P. Benech, *et al.*, "Wavelength-scale stationary-wave integrated Fourier-transform spectrometry," Nat. Photonics **1**, 473 (2007).
10. N. Cvetojevic, N. Jovanovic, J. Lawrence, *et al.*, "Developing arrayed waveguide grating spectrographs for multi-object astronomical spectroscopy," Opt. Express **20**, 2062 (2012).
11. N. Cvetojevic, J. S. Lawrence, S. C. Ellis, *et al.*, "Characterization and on-sky demonstration of an integrated photonic spectrograph for astronomy," Opt. Express **17**, 18643 (2009).
12. N. Cvetojevic, N. Jovanovic, C. Betters, *et al.*, "First starlight spectrum captured using an integrated photonic micro-spectrograph," Astron. Astrophys. **544**, L1 (2012).
13. N. Jovanovic, N. Cvetojevic, B. Norris, *et al.*, "Demonstration of an efficient, photonic-based astronomical spectrograph on an 8-m telescope," Opt. Express **25**, 17753 (2017).
14. A. Stoll, K. V. Madhav, and M. M. Roth, "Design, simulation and characterization of integrated photonic spectrographs for astronomy: generation-I AWG devices based on canonical layouts," Opt. Express **29**, 24947 (2021).
15. A. Stoll, K. Madhav, and M. Roth, "Design, simulation and characterization of integrated photonic spectrographs for astronomy II: low-aberration Generation-II AWG devices with three stigmatic points," Opt. Express **29**, 36226 (2021).
16. Y. Zhang, J. Zhan, S. Veilleux, *et al.*, "Arrayed waveguide grating with reusable delay lines (RDL-AWG) for high resolving power, highly compact, photonic spectrographs," in *2022 IEEE Photonics Conference (IPC)* (2022), p. 1.
17. A. C. van Wijk, C. R. Doerr, and I. B. Akca, "Custom arrayed waveguide gratings with improved performance," Adv. Photon. Res. **4**, 2300198 (2023).
18. K. Takada and M. Abe, "UV trimming of AWG devices," in *Bragg Gratings, Photosensitivity, and Poling in Glass Waveguides*, Technical Digest (2003), p. TuA1.
19. A. Stoll, Z. Zhang, and R. Haynes, "High-resolution arrayed-waveguide-gratings in astronomy: design and fabrication challenges," Photonics **4**, 30 (2017).
20. P. Gatkine, N. Jovanovic, C. Hopgood, *et al.*, "Potential of commercial SiN MPW platforms for developing mid/high-resolution integrated photonic spectrographs for astronomy," Appl. Opt. **60**, D15 (2021).
21. J. Liu, H. Tian, E. Lucas, *et al.*, "Monolithic piezoelectric control of soliton microcombs," Nature **583**, 385 (2020).
22. M. Gehl, D. Trotter, A. Starbuck, *et al.*, "Active phase correction of high resolution silicon photonic arrayed waveguide gratings," Opt. Express **25**, 6320 (2017).
23. Y. Zhang, A. Samanta, K. Shang, *et al.*, "Scalable 3D silicon photonic electronic integrated circuits and their applications," IEEE J. Sel. Top. Quantum Electron. **26**, 8201510 (2020).